metals

MDPI

Article

An Approach for Modelling Slag Infiltration and Heat Transfer in Continuous Casting Mold for High Mn–High Al Steel

Jie Yang *, Dengfu Chen *, Mujun Long and Huamei Duan

College of Materials Science and Engineering, Chongqing University, Chongqing 400044, China; longmujun@cqu.edu.cn (M.L.); duanhuamei@cqu.edu.cn (H.D.)

* Correspondence: yangjie2018@cqu.edu.cn (J.Y.); chendfu@cqu.edu.cn (D.C.); Tel.: +86-133-2246-6016 (J.Y.); +86-023-6510-2467 (D.C.)

Received: 22 November 2019; Accepted: 24 December 2019; Published: 26 December 2019

Abstract: To clarify the characteristics of slag infiltration and heat transfer behaviors in the meniscus region during the casting of high Mn–high Al steel, a mathematical model of a continuous casting mold that couples fluid flow with heat transfer, and solidification is developed. The model is based on the change in slag composition and properties caused by the steel/slag reaction. The formation and evolution of the meniscus profile and slag films for different mold fluxes during mold oscillation are described. The results show that the rapid growth of the slag rim with a high Al_2O_3 content approaches and deforms the meniscus so that a series of casting problems such as slag infiltration blocking, large fluctuations in heat flux, and even meniscus breaking occur in the continuous casting process. Predictions are in good agreement with plant measurements. These findings provide an improved understanding of the complex phenomena occurring in the meniscus region and give new insights into the evaluation and optimization of mold flux properties for high Mn–high Al steel casting.

Keywords: high Mn–high Al steel; continuous casting mold; slag infiltration; heat transfer

1. Introduction

High Mn–high Al steel is widely used as wear-resistant, non-magnetic, lightweight automobile, and ocean platform steel due to its outstanding mechanical properties such as high tensile strength, extraordinary ductility, and excellent work hardening ability. However, the strong interfacial reaction between high Al–high Mn steel and mold flux occurs in the mold during the casting process. Kim and Park [1] found that the content of Al and Si in the molten steel changes rapidly in the first 15 min of the interfacial reaction through the investigation of reaction kinetics and related phenomena. It is known that the slag powder on the top of molten steel is heated and melted to generate a liquid pool. The liquid slag from the pool infiltrates into a narrow gap between the solidified shell and the mold to form two layers of slag film under the influence of mold oscillation. The thickness and distribution of the slag films have a significant impact on the heat transfer and lubrication of the slab. During the continuous casting of high Mn–high Al steel, the change of the slag composition, which mainly embodies Al_2O_3 accumulation coupled with SiO_2 reduction, deteriorates lubrication and heat transfer conditions in the mold, thus inducing various kinds of casting problems such as transverse and longitudinal cracks, depressions, and breakout alarms, as reported by Blazek et al. [2]. The properties of mold flux have been some of the most important factors that have limited the high-efficiency continuous casting of high Mn–high Al steel.

Some studies have been conducted to reveal the reaction phenomena that take place at the interface between molten steel with high Mn–high Al-containing and CaO–SiO_2-based mold fluxes. The Al

content in molten steel has been regarded as the key factor that controls the interfacial reaction and results in the Al_2O_3 accumulation in the mold flux, as stated by Kim et al. [3]. Zhang et al. [4] indicated that the Al_2O_3 content in the mold flux accumulates rapidly within a short period of the casting process, and the viscosity increases with the increasing w (Al_2O_3)/w (SiO_2). In a study by Ryu et al. [5], increases of basicity and Al_2O_3 content promoted the crystallization tendency of the mold flux, which resulted in the formation of a large slag rim that obstructed the slag infiltration. In this case, some optimizations were conducted to solve those problems by adding fluxing agents like B_2O_3 and Li_2O, as investigated by Seo et al. [6]. On the other hand, intensive attempts have been carried out to develop and assess the CaO–Al_2O_3-based mold flux system, which avoids the negative effects of slag properties caused by the pickup of Al_2O_3 [7–9]. Shi et al. [10] evaluated the effects of crystallization characteristics of lime–alumina based mold fluxes on lubrication and heat transfer. Recent studies focusing on the effect of additives on melting and heat transfer of CaO–Al_2O_3-based mold flux have been proposed by Zhou et al. [11] in case of LiO_2 and by Yang et al. [12] for B_2O_3. However, previous research on the mold flux for high Mn–high Al steel has mainly focused on the testing and the adjustment of macroscopic properties for adapting casting conditions. There have been few considerations for the differences in the properties of mold flux in the mold when casting steels with different Mn and Al contents. Furthermore, the dynamic lubrication and heat transfer phenomena of mold flux during mold oscillation have not been studied.

In our previous work, a numerical model that addresses the limitations of concurrent phenomena in the continuous casting mold, including fluid flow, heat transfer, shell solidification and mold oscillation, was developed [13,14]. The model was successfully used to characterize the slag infiltration phenomena and initial shell solidification during the casting process from cast-start to steady-state. In the current study, the mathematical model is applied in combination with an interfacial reaction experiment to describe the formation and evolution of the meniscus profile and slag films in a continuous casting mold for high Mn–high Al steel. The model predictions were used to gain insight into the change features of slag infiltration and heat transfer in the mold and to evaluate the performance of mold flux during the high Mn–high Al steel casting. The aim of this study is to provide a new perspective for the design and optimization of mold flux for high Mn–high Al steel.

2. Model Development

2.1. Model Description

The mathematical model developed in this study consisted of a fluid flow model, a heat transfer coupled with solidification model, and a mold oscillation model. The volume of fluid (VOF) method and the continuum surface force (CSF) model were coupled to the Navier–Stokes equations to solve the steel and slag flow and track their interface.

$$\frac{\partial}{\partial t}(\alpha_{\text{steel}}\rho_{\text{steel}}) + \nabla\cdot\left(\alpha_{\text{steel}}\rho_{\text{steel}}\vec{v}\right) = S_{\alpha_{\text{steel}}} + \sum\left(\dot{m}_{\text{slag-steel}} - \dot{m}_{\text{steel-slag}}\right) \tag{1}$$

$$\frac{\partial}{\partial t}\left(\rho_{\text{mix}}\vec{v}\right) + \nabla\cdot\left(\rho_{\text{mix}}\vec{v}\vec{v}\right) = -\nabla p + \nabla\cdot\left[\mu_{\text{mix}}\left(\nabla\vec{v} + \nabla\vec{v}^{T}\right)\right] + \rho_{\text{mix}}\vec{g} + \vec{F}_{\sigma} \tag{2}$$

where α is the phase fraction, ρ is the density, $\vec{v}$ is the velocity vector, p is the pressure, $\vec{g}$ is the gravitational force vector, $\dot{m}$ is the mass transfer between the phases, and $\vec{F}_{\sigma}$ is the momentum sink due to the interfacial tension between steel and slag, which is expressed as:

$$\vec{F}_{\sigma} = \sigma_{\text{slag-steel}}\frac{\rho_{\text{mix}}\kappa\nabla\alpha_{\text{slag}}}{\frac{1}{2}\left(\rho_{\text{slag}} + \rho_{\text{steel}}\right)} \tag{3}$$

where $\sigma_{\text{slag-steel}}$ is the interfacial tension between steel and slag and κ is the local surface curvature.

The effect of turbulence in the fluid region is predicted by using the realizable k-ε model, and the heat transfer is calculated based on the Fourier equation. The solid matter in the mushy and solidified regions is treated as a porous medium by the enthalpy–porosity technique,

$$S_{\mathrm{m}} = \frac{(1-\beta)^2}{(0.001+\beta^3)} A_{\mathrm{mush}} \left(\vec{v} - \vec{v}_{\mathrm{pull}}\right) \tag{4}$$

where β is the liquid volume fraction, A_{mush} is the mushy zone constant, and $\vec{v}_{\mathrm{pull}}$ is the pulling velocity. The details about governing the equations of the coupling model were published in our previous work [13].

The boundary conditions and model domain are shown in Figure 1. The two-dimensional mold model domain included a half SEN (submerged entry nozzle) with outlet ports angled 15 degrees downward, a half mold of 0.825 m in width, and 1 m of slab below the exit of the mold. A velocity inlet condition was applied at the SEN top to maintain the mass balance according to the casting speed. Molten steel entered the mold through the nozzle port that is submerged 0.152 m below the metal level. The addition of a 50 mm thick slag bed on the liquid steel surface allowed for the calculation of the liquid pool and the sintered layer through the solidification temperature isotherm, including a slag rim adhered to the oscillating mold. The calculation of the slag rim corresponded to liquid slag that had returned to solid state in the mold corner. A pressure inlet condition with a constant temperature of 313 K was applied at an air zone top, which was added as the atmosphere on the surface of the mold flux. The heat extracted by the mold was solved through the convective heat transfer of the cooling water. The heat transfer between the mold and the molten steel was determined by the formation of slag films that were not predefined but result from slag infiltration. The mold domain was defined by a sinusoidal oscillation mode that was specified as a function of the frequency and the stroke. The interface between the mold domain and the steel was coupled in both velocity and heat transfer. The secondary cooling region was modeled as a combined convection with an external radiation boundary condition. Heat flux through the SEN walls was assumed to be zero. The casting parameters used in this calculation are listed in Table 1. The multiphysics behaviors were solved simultaneously for a period of time to obtain the steady shell growth and slag infiltration [14].

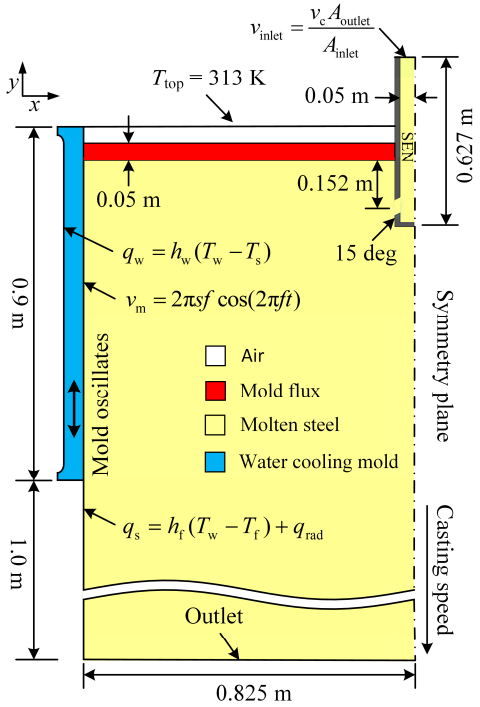

Figure 1. Schematic of model domain and boundary conditions.

Table 1. Parameters used in the simulation.

Parameter	Value
Superheat temperature/°C	25
Casting speed/(m/min)	1.2
Water temperature/°C	30
Amplitude/mm	2.5
Frequency/(min^{-1})	152

2.2. Compositions and Properties of Slag

Slag properties are determined by the combinations of individual components, and these properties evolve during the continuous casting process, especially the casting for high Mn–high Al steel due to the steel/slag reaction. Therefore, the evolution of slag composition during the interfacial reaction with different contents of Mn and Al steel was firstly examined through a laboratory reaction experiment, and the results are shown in Figure 2. A detailed experimental procedure was described in our previous work [15]. It could be seen from the experiment that the main reaction occurring at the interface was the reduction of SiO_2 by the Al in the molten steel, resulting in the significant SiO_2 reduction and Al_2O_3 accumulation in the mold flux. The continuous increase in MnO content was only observed when 0.8% Al-containing steel was applied. Instead, the amount of MnO showed a downward trend after the first rise during the reaction with 1.5% Al-containing steel because the MnO formed in the mold flux was reduced again by the excess Al in the molten steel. Therefore, the final slag compositions after the reaction were significantly different according to the contents of Mn and Al in the molten steel. Based on the experimental results, the compositions of slag samples used in the simulation are given in Table 2, including an initial slag composition (M1) and three final slag compositions (M2, M3, and M4).

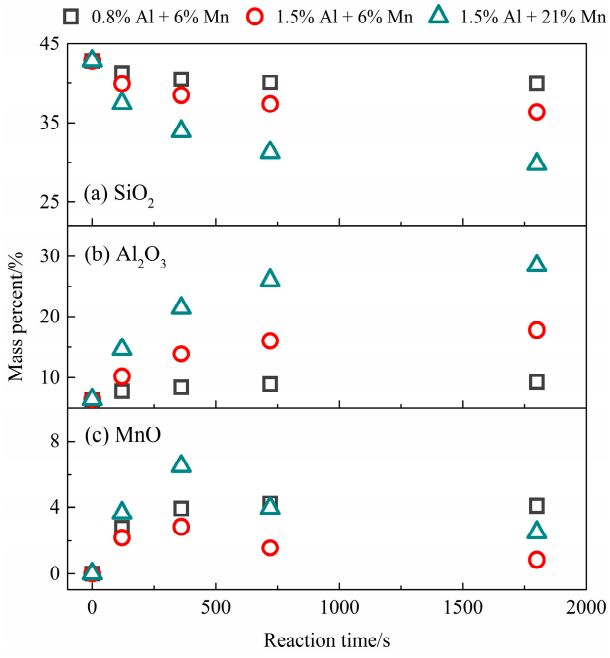

Figure 2. Evolution of slag composition during the interfacial reaction.

Table 2. Mold slag composition (mass percent).

Samples	CaO	SiO_2	Al_2O_3	MgO	Na_2O	F	MnO
M1	33.15%	42.82%	6.41%	2.24%	8.86%	6.51%	0%
M2	31.83%	39.96%	9.32%	2.15%	8.51%	6.25%	4.08%
M3	31.33%	36.36%	17.82%	2.11%	8.38%	6.15%	0.83%
M4	29.75%	29.78%	28.39%	2.01%	7.95%	5.84%	2.50%

The slag properties were estimated by using the measurements and the previous models according to the slag composition, which varied as a function of the temperature. It is known that slag viscosity increases gradually with the decreasing temperature and suddenly increases at its break temperature [16]. In the current model, the viscosity–temperature curve above the break temperature of each mold slag was drawn according to the measured data. Then, the viscosity below the break temperature was defined as two-stage linear growth, and the maximum viscosity was truncated at 10^4 Pa s to avoid numerical problems [17], as shown in Figure 3.

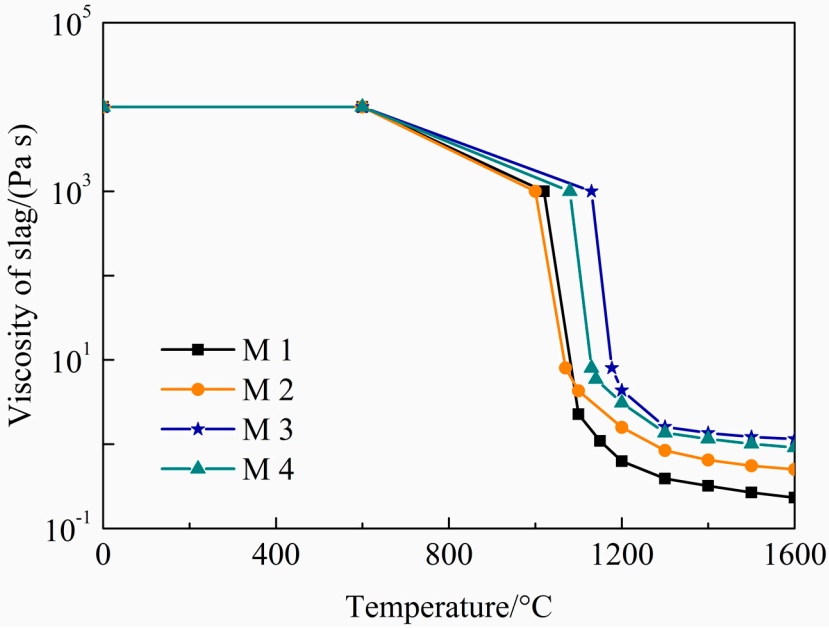

Figure 3. Viscosity–temperature curves of mold slag.

The effective thermal conductivity that was comprised of conduction and radiation was adopted in the calculations. Above the melting temperature, a constant thermal conductivity of 3 W/m K was used for the initial slag, which is consistent with the measurement of Hasegawa et al. [18]. As the thermal conductivity of molten slag increased with increasing SiO_2 content, a moderate decrease of the thermal conductivity in final slags was adopted according to the slag compositions [19]. Below the solidification temperature, the effective thermal conductivity for solid state was given between 0.6 and 1.0 W/m K based on the model of McDavid and Thomas [20], as shown in Figure 4. The other constants of material property in model calculation are listed in Table 3.

Table 3. Constants of material property.

Properties for High Mn–High Al Steel				
Liquidus Temperature/°C	1421			
Solidus Temperature/°C	1378			
Latent heat/(kJ/kg)	315			
Slag Properties				
	M1	**M2**	**M3**	**M4**
Solidification temperature/°C	1117	1195	1222	1199
Viscosity at 1300 °C/(Pa s)	0.391	0.842	1.362	1.608
Slag/steel interfacial tension/(N/m)	1.33	1.35	1.34	1.36

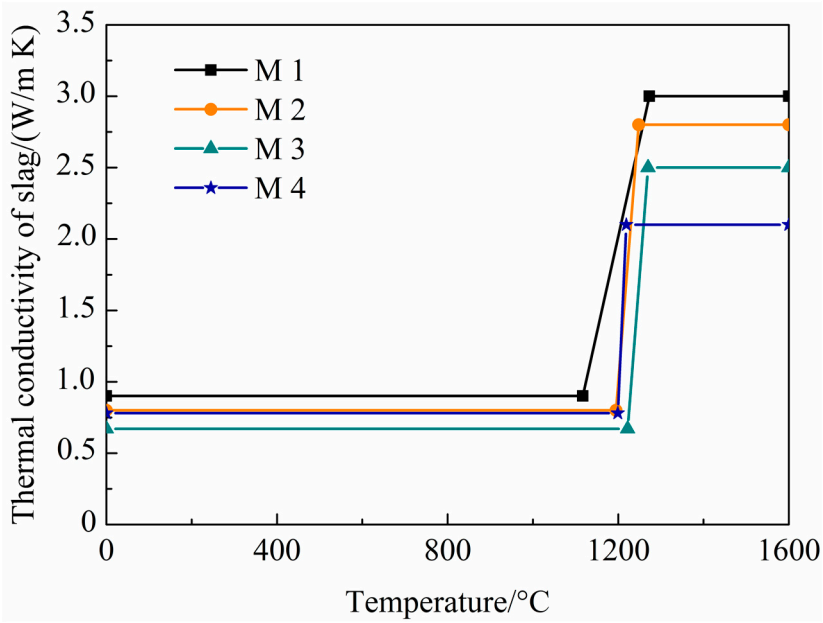

Figure 4. Thermal conductivity–temperature curves of mold slag.

3. Results and Discussion

3.1. Formation of Slag Films

The initial solidification of steel arose along the steel/slag interface close to the cooling mold, forming a shell tip, which was withdrawn at the casting speed. Complex and intense metal and slag flow, heat transfer and solidification behaviors occurred simultaneously in the meniscus region. During the casting of the high Mn–high Al steel, the change in slag composition had a decisive influence on the heat transfer and lubrication conditions between the mold and the solidified shell, which was responsible for the formation of defects during the solidification. Figure 5 shows the model predictions in the meniscus region for different mold fluxes, including the meniscus profile, liquid slag film thickness, solid slag film thicknesses, and mold temperature distribution. For comparison, the meniscus and slag film formed using the initial slag (without the steel/slag reaction) are shown in Figure 5a. As the solidification temperature of mold flux increased, the thickness of solid slag film increased. Meanwhile, a narrow channel of slag infiltration in the meniscus was formed, and this was where a larger hydraulic pressure acted on the meniscus surface to generate a depression during the mold oscillation, as presented in Figure 5b. Obviously, the larger slag rim and the narrower flux channel deepened the surface defects on the slab. This situation was more serious in the process shown in Figure 5c,d, when the Al_2O_3 content in the M3 and M4 slags reached 17.82% and 28.39%, respectively. The large slag rim formed by the high viscosity and solidification temperature can be directly pressed to the meniscus during the oscillation process, which leads to the overflow of molten steel to form severe hook-type oscillation marks or induces breakout—this is the reason that the slag rim is continuously removed to avoid the casting problem in the practice of high Mn–high Al steel casting.

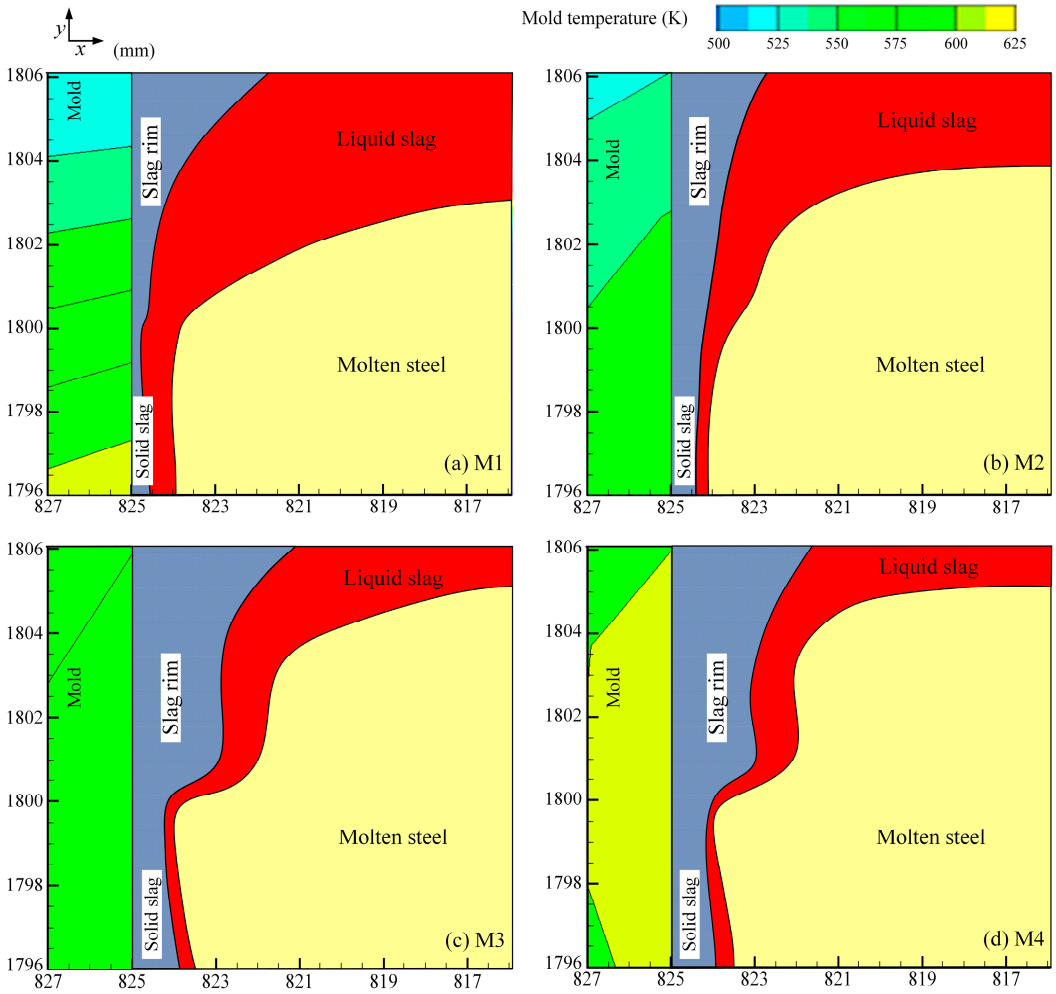

Figure 5. Model predictions in meniscus region.

The formation of solid slag film contributed to stabilize the horizontal heat transfer, while the liquid slag formed a lubrication channel to avoid sticking of the solidified shell to the mold. In order to compare the effects of slag components on the formation of slag films, the solid and liquid slag film thicknesses of four types of mold flux are shown Figure 6. The solidification temperature of mold flux increased with the increasing basicity and Al_2O_3 content in the acidic slag; thus, the solid slag film thickness gradually increased in the M1, M2 and M3 slags, and the increase in the M3 slag was larger. As a network former, Al_2O_3 increased the ionic polymerization degree to slow the molecular migration and crystal nucleation in the M4 slag when its content reached 28.39%, which made the solidification temperature drop a little. Therefore, the solid slag film thickness of the M4 slag presented a slight decrease, while the thickness of liquid slag film continued to decrease. Note that despite the large difference in Al_2O_3 content in the mold flux, the slag film thicknesses of the M3 and M4 slags were relatively close.

To verify the model predictions, the calculated slag rim profiles of the M1 and M3 slags were compared with those of the conventional steel grade and high Al steel (0.8% Al) in plant trials, as shown in Figure 7. The Al_2O_3 accumulation in the slag rim from the plant trials of the high Al steel was 20.17%, which was slightly higher than that in the M3 slag. It can be seen that the slag rim thickness of the M1 slag was less than 5 mm without the occurrence of steel/slag reaction, which was more than doubled in the M3 slag with a high amount of Al_2O_3. The predicted shapes of the slag rim were similar to that obtained from the two types of steels during the casting practice. It is worth noting that since a small portion of the liquid slag and the powder adhered to the edge when the slag rim was taken out

from the continuous casting mold, the edge of slag rim was rough and slightly thicker than the state inside the mold.

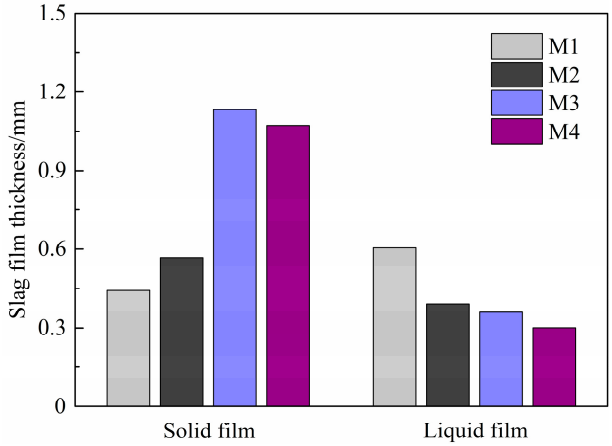

Figure 6. Solid and liquid slag film thicknesses.

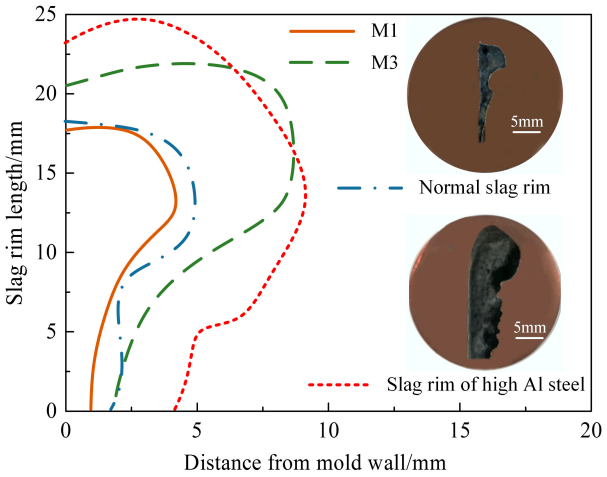

Figure 7. Comparison of calculated slag rim profiles to plant measurements.

3.2. Evolution of Slag Infiltration and Heat Flux

During the casting of high Mn–high Al steel, the rapid formation of a large slag rim and the high viscosity of mold flux are detrimental to slag infiltration, resulting in uneven and discontinuous slag film, which seriously deteriorates the heat transfer and lubrication conditions in the mold. Therefore, the current study focused on the variation of the relative distance between the slag rim and the meniscus throughout the oscillation process, as presented in Figure 8. It should be noted that this distance was measured from the solidification tip at the meniscus to the lower edge of the slag rim directly above. The thick solid lines in the figure were the average distance between the slag rim and the meniscus in four cases, and the thin dotted lines were the actual distance corresponding to the amplitude of mold oscillation. The distance between the slag rim and the meniscus gradually shrunk in the beginning of model calculations. The growth rate of slag rim slowed after 5 s when the M1 and M2 slags were applied; thus, the distance tended to be stable. On the other hand, the slag rim from the M3 and M4 slags grew faster so that the slag rim contacted the meniscus surface when the mold moves downward after 5 s, which caused a series of casting problems such as slag infiltration blocking and meniscus breaking. It should be noted that the composition of mold flux changes continuously with the reaction in the casting practice, so its properties tend to be stable after 10–15 min of casting, as reported by Fu et al. [21]. However, the properties of mold flux used in this model calculations were fixed, which was determined by the composition obtained from the results of steel/slag reaction experiment.

Therefore, the growth rate of slag rim in the numerical calculations is significantly higher than the actual situation, but the final size is consistent with the plant measurement, as shown in Figure 7. Thus, the model predictions can be considered credible, which is beneficial to understand the obstruction phenomenon of slag infiltration caused by the large slag rim during the high Mn–high Al steel casting.

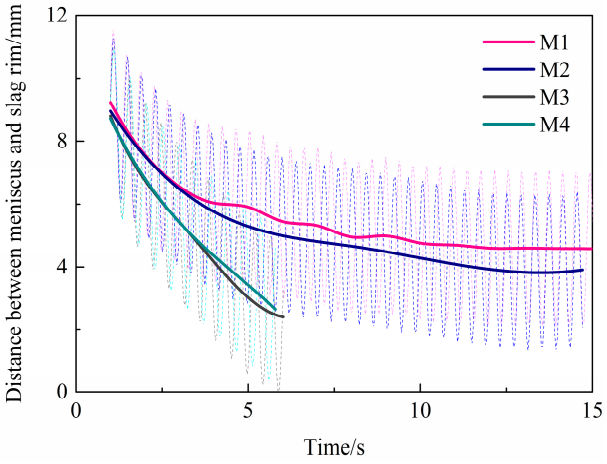

Figure 8. Distance between meniscus and slag rim as a function of time.

It is well known that slag consumption is an important indicator for evaluating the lubrication conditions in a mold. Figure 9 shows the average consumption of mold flux as a function of time and the plant measurement of high Al steel (0.8% Al) for comparison. Obviously, the slag consumption decreased with the decreasing thickness of liquid slag under the influence of the steel/slag reaction. Since the liquid slag film of the M3 and M4 slags was thinner and more viscous, the average consumption was lower, and the rate of decline was faster. As discussed above, the inflow channel of the liquid slag was blocked when the large slag rim with a high Al_2O_3 content approached the meniscus, causing the slag consumption to drop to a low level. The average slag consumption in the casting practice was maintained at about 0.35 kg/m^2 by constantly removing the slag rim, a consumption that was slightly higher than the steady consumption of the M2 slag in the model calculation.

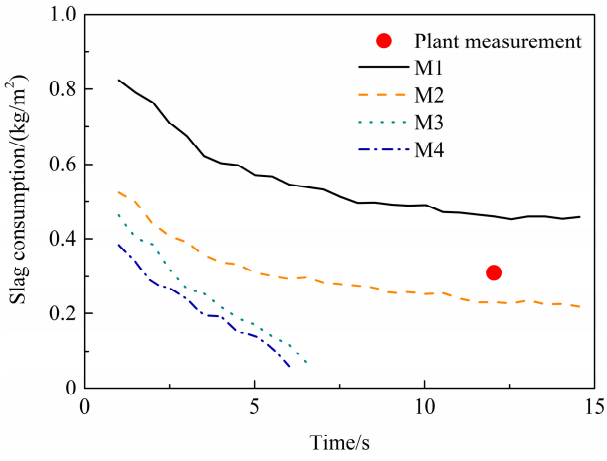

Figure 9. Slag consumption as a function of time.

The solid slag film formed between the mold and the solidified shell controlled the horizontal heat transfer in the mold. Periodic fluctuations of the heat flux were produced by the mold oscillation, which affected the initial shell solidification. Figure 10 presents the heat flux evolution at the meniscus. It can be seen that since the solid slag films formed by the M1 and M2 slags were thin, and the average heat fluxes at the meniscus were slightly higher than that of the M3 and M4 slags. The heat flux of the

M1 and M2 slags greatly fluctuated during the initial growth of the slag film, and then the fluctuation amplitude gradually decreased and tended to be stable. A high fluctuation in the heat flux of the M2 slag was detected due to the disturbance of the liquid level by the slag rim. This phenomenon was more prominent in the M3 and M4 slags, as shown in Figure 10c,d. The rapid growth of the slag rim quickly approached the meniscus, resulting in an enhanced convective heat transfer at the meniscus. Thus, the overall heat flux rose while the fluctuation became more intense. This was also reflected in the temperature distribution of the mold copper in Figure 5. It can be seen that the mold temperature near the meniscus was abnormally increased and was accompanied by the expansion of the high temperature zone, which is an important signal for judging the occurrence of breakout. Therefore, the simulation method proposed in this study can be used to predict the formation and evolution of the meniscus profile and slag films during the casting process of high Mn–high Al steel and to evaluate the performance of mold flux through the characteristics of slag infiltration and heat transfer in the mold. The purpose of this study is to provide the guidance for the design and assessment of the mold flux used for high Mn–high Al steel casting.

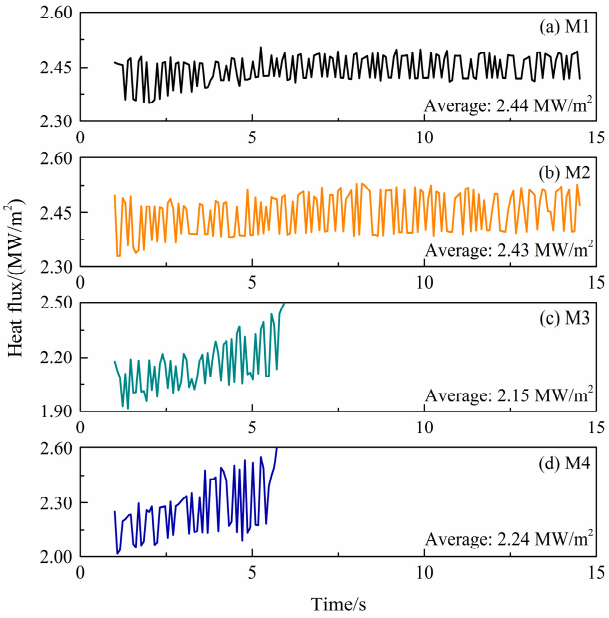

Figure 10. Heat flux as a function of time.

4. Conclusions

A numerical model that couples the multiphase flow with heat flux and solidification in a continuous casting mold for high Mn–high Al steel has been developed. The model is used to characterize slag infiltration and heat transfer in the meniscus region with different mold fluxes. The results show that as the Al_2O_3 accumulation in the mold flux increases, the flux channel becomes narrower, while the thickness of solid slag film rapidly increases and then slightly decreases due to the decrease of solidification temperature. The growth of the slag rim produces a greater pressure that acts on the meniscus surface to generate a depression during the mold oscillation. The large slag rim with a high Al_2O_3 content quickly approaches the meniscus, which results in a series of casting problems such as slag infiltration blocking, large fluctuations in heat flux, and even meniscus breaking.

The model developed in this study correctly predicts the formation of the meniscus profile and slag films during the casting process of high Mn–high Al steel, and it shows good agreement with plant measurements. These results provide new insights into the evaluation of mold flux properties for high Mn–high Al steel casting.

Author Contributions: Conceptualization, J.Y. and D.C.; investigation, J.Y.; methodology, J.Y. and M.L.; data curation, J.Y. and H.D.; writing—original draft preparation, J.Y.; supervision, D.C. All authors have read and agreed to the published version of the manuscript.

Funding: This research was funded by the National Natural Science Foundation of China (grant numbers 51904046 and 51874060) and the Postdoctoral Science Foundation of Chongqing (grant number cstc2019jcyj-bshX0027).

Conflicts of Interest: The authors declare no conflict of interest.

References

1. Kim, D.J.; Park, J.H. Interfacial reaction between CaO-SiO_2-MgO-Al_2O_3 flux and Fe-xMn-yAl (x = 10 and 20 mass pct, y = 1, 3, and 6 mass pct) steel at 1873 K (1600 °C). *Metall. Mater. Trans. B* **2012**, *43*, 875–886. [CrossRef]
2. Blazek, K.; Yin, H.; Skoczylas, G.; McClymonds, M.; Frazee, M. Development and evaluation of lime alumina-based mold powders for casting high-aluminum TRIP steel grades. *Iron Steel Technol.* **2011**, *8*, 232–240.
3. Kim, M.; Lee, S.; Cho, J.; Park, M.; Lee, H.; Kang, Y. A reaction between high Mn-high Al steel and CaO-SiO_2-type molten mold flux: Part I. Composition evolution in molten mold flux. *Metall. Mater. Trans. B* **2013**, *44*, 299–308. [CrossRef]
4. Zhang, Z.; Wen, G.H.; Tang, P. The influence of Al_2O_3/SiO_2 ratio on the viscosity of mold fluxes. *ISIJ Int.* **2008**, *48*, 739–746. [CrossRef]
5. Ryu, H.G.; Zhang, Z.T.; Cho, J.W.; Wen, G.H.; Sridhar, S. Crystallization behaviors of slags through a heat flux simulator. *ISIJ Int.* **2010**, *50*, 1142–1150. [CrossRef]
6. Seo, M.; Shi, C.; Cho, J.; Kim, S. Crystallization behaviors of CaO-SiO_2-Al_2O_3-Na_2O-CaF_2-(Li_2O-B_2O_3) mold fluxes. *Metall. Mater. Trans. B* **2014**, *45*, 1874–1886. [CrossRef]
7. Wu, T.; Wang, Q.; He, S.P.; Xu, J.F.; Long, X.; Lu, Y.J. Study on properties of alumina-based mould fluxes for high-Al steel slab casting. *Steel Res. Int.* **2012**, *83*, 1194–1202. [CrossRef]
8. Cho, J.; Blazek, K.; Frazee, M.; Yin, H.B.; Park, J.H.; Moon, S.W. Assessment of CaO-Al_2O_3 based mold flux system for high aluminum TRIP casting. *ISIJ Int.* **2013**, *53*, 62–70. [CrossRef]
9. Yan, W.; Chen, W.; Yang, Y.; Lippold, C.; McLean, A. Effect of CaO/Al_2O_3 ratio on viscosity and crystallization behaviour of mould flux for high Al non-magnetic steel. *Ironmak. Steelmak.* **2015**, *42*, 698–704. [CrossRef]
10. Shi, C.; Seo, M.; Cho, J.; Kim, S. Crystallization characteristics of CaO-Al_2O_3-Based mold flux and their effects on in-mold performance during high-aluminum TRIP steels continuous casting. *Metall. Mater. Trans. B* **2014**, *45*, 1081–1097. [CrossRef]
11. Zhou, L.; Li, H.; Wang, W.; Xiao, D.; Zhang, L.; Yu, J. Effect of Li_2O on the behavior of melting, crystallization, and structure for CaO-Al_2O_3-based mold fluxes. *Metall. Mater. Trans. B* **2018**, *49*, 2232–2240. [CrossRef]
12. Yang, J.; Zhang, J.; Ostrovski, O.; Zhang, C.; Cai, D. Effects of B_2O_3 on crystallization, structure, and heat transfer of CaO-Al_2O_3-based mold fluxes. *Metall. Mater. Trans. B* **2019**, *50*, 291–303. [CrossRef]
13. Yang, J.; Cai, Z.; Zhu, M. Transient thermo-fluid and solidification behaviors in continuous casting mold: Evolution phenomena. *ISIJ Int.* **2018**, *58*, 299–308. [CrossRef]
14. Yang, J.; Meng, X.; Zhu, M. Transient thermo-fluid and solidification behaviors in continuous casting mold: Oscillation behaviors. *ISIJ Int.* **2018**, *58*, 2071–2078. [CrossRef]
15. Yang, J.; Zhu, M. Evolution of compositions and properties of CaO-SiO_2 based mold flux for continuous casting high Mn steel. *ISIJ Int.* **2016**, *56*, 2191–2198. [CrossRef]
16. Mills, K.C.; Fox, A.B.; Li, Z.; Thackray, R.P. Performance and properties of mould fluxes. *Ironmak. Steelmak.* **2005**, *32*, 26–34. [CrossRef]
17. Jonayat, A.; Thomas, B.G. Transient thermo-fluid model of meniscus behavior and slag consumption in steel continuous casting. *Metall. Mater. Trans. B* **2014**, *45*, 1842–1864. [CrossRef]
18. Hasegawa, H.; Ohta, H.; Shibata, H.; Waseda, Y. Recent development in the investigation on thermal conductivity of silicate melts. *High Temp. Mater. Proc.* **2012**, *31*, 299–673. [CrossRef]
19. Hayashi, M.; Ishii, H.; Susa, M.; Fukuyama, H.; Nagata, K. Effect of ionicity of nonbridging oxygen ions on thermal conductivity of molten alkali silicates. *Phys. Chem. Glasses* **2001**, *42*, 6–11.

20. McDavid, R.M.; Thomas, B.G. Flow and thermal behavior of the top surface flux powder layers in continuous casting molds. *Metall. Mater. Trans. B* **1996**, *27*, 672–685. [CrossRef]
21. Fu, X.J.; Wen, G.H.; Liu, Q.; Tang, P.; Li, J.Z.; Li, W. Development and evaluation of CaO-SiO_2 based mould fluxes for casting high Aluminum TRIP steel. *Steel Res. Int.* **2014**, *86*, 110–120. [CrossRef]